Semiconductor Physics, Quantum Electronics & Optoelectronics, 2025. V. 28, No 4. P. 441-448.

Hetero- and low-dimensional structures

Tailoring structural and optical properties of Si-doped HfO_2 thin films via target composition and plasma environment

D.V. Khomenkov[1,*], S.S. Ponomaryov[2], X. Portier[3], L.Yu. Melnichuk[1], L.Yu. Khomenkova[2,4], F. Gourbilleau[3], O.V. Melnichuk[1,]**

[1]*Mykola Gogol State University of Nizhyn, 2 Grafska Street, 16600 Nizhyn, Ukraine*
[2]*V. Lashkaryov Institute of Semiconductor Physics, NAS of Ukraine, 41 Nauky Avenue, 03028 Kyiv, Ukraine*
[3]*CIMAP/CEA/CNRS/ENSICAEN/UCBN, 6 Boulevard Marechal Juin, 14000 Caen, France*
[4]*National University "Kyiv Mohyla Academy", 2 Skovorody Street, 04070 Kyiv, Ukraine*
Corresponding author e-mail: khomenkov.dv@ndu.edu.ua, dmkhomen@gmail.com[*]; mov310310@gmail.com[**]

Abstract. Optical and structural properties of as-deposited Si-doped HfO_2 thin films were investigated as a function of target composition, substrate temperature (100…500 °C), and plasma environment. The films were deposited on Si (100) substrates by RF magnetron sputtering from composite Si:HfO_2 targets in either pure argon or argon–hydrogen plasma. The Si content in the films was varied by adjusting the target composition, the hydrogen fraction in the plasma, and the total pressure. TEM, FTIR, ellipsometry, and Auger electron spectroscopy revealed that the Si-doped films maintained chemical uniformity and dense amorphous structure. For deposition in pure Ar plasma at a total pressure of 0.04 mbar, increasing Si incorporation led to formation of homogeneous amorphous films with a refractive index higher than that of pure HfO_2 (2.42 vs. 1.98 at 1.95 eV). Deposition in Ar-H_2 plasma enabled further raise of the refractive index up to 2.75 through variation of the hydrogen flow rate. An even higher refractive index up to 3.4 was achieved by lowering the total pressure to 0.02 mbar and/or by increasing the substrate temperature. However, the latter resulted in a reduced film growth rate. The extended structure–zone model provided a consistent framework to interpret the observed film morphologies, linking adatom mobility, ion bombardment, and film densification to the deposition parameters. The novelty of this work is in demonstrating that hydrogen-assisted reactive sputtering enables *in situ* control of the Si content during deposition without need to modify the target composition. These findings show that the microstructure and optical response of Si-doped HfO_2 films can be systematically tailored, offering a route for designing high-index amorphous coatings suitable for optical and microelectronic applications.

Keywords: HfO_2, Si-doped HfO_2, magnetron sputtering, thin films, ellipsometry, FTIR, TEM, Auger spectroscopy.

https://doi.org/10.15407/spqeo28.04.441
PACS 68.37.Lp, 78.66.-w, 78.20.-e, 81.15.Cd

Manuscript received 21.09.25; revised version received 06.11.25; accepted for publication 26.11.25; published online 15.12.25.

1. Introduction

Hafnium oxide (HfO_2) and its stoichiometric silicate ($HfSiO_4$) are gaining prominence as potential replacements of SiO_2 in microelectronics owing to their high thermal and chemical stability, low tunneling current and excellent compatibility with silicon-based channels [1]. Both HfO_2 and $HfSiO_4$ have higher refractive indices as compared to SiO_2, which makes them attractive materials for optical waveguides application [2]. However, the relatively low crystallization temperature of HfO_2 (300…350 °C) [3] and the tendency of $HfSiO_4$ to undergo phase separation at elevated temperatures [4, 5] critically influence their performance. Consequently, achieving amorphous structural stability and compositional uniformity at high temperatures remains a major challenge.

Among various film fabrication techniques, magnetron sputtering is a physical vapor deposition process that enables film growth under non-equilibrium conditions [6–9]. Radio-frequency (RF) magnetron sputtering is particularly promising for deposition of dielectric HfO_2-based films, as it allows precise control over their chemical composition, homogeneity, and structure [7–12]. The structure of the HfO_2-based films strongly depends on the deposition conditions such as the cathode power, target-to-substrate distance, substrate temperature, chamber pressure, gas composition (argon mixed with oxygen, nitrogen, or hydrogen), and post-deposition annealing [8–16].

In our earlier studies, we proposed an approach to improve the stability of the amorphous structure in thin HfO_2 films [8, 9]. For ultrathin (< 10 nm) films, this stabilization was attributed to the high surface-to-volume ratio and elevated surface energy. For thicker films, doping with 3 at.% Si preserved the amorphous structure up to 800 °C [9]. Later, structural stability was also reported for thicker films doped with ~12 at.% Si grown in pure Ar plasma [9, 12, 13]. However, to gain a deeper understanding of how Si doping influences optical and structural properties of HfO_2-based films, a comprehensive investigation covering a wide range of Si contents was required.

It is known that deposition in pure argon plasma allows fabrication of films with a chemical composition closely matching that of the sputtered target [6, 7, 13, 14]. Sputtering a HfO_2 target in an argon–oxygen mixture promotes Hf oxidation, leading to formation of stoichiometric hafnium dioxide [15].

Si-doped HfO_2 films are typically obtained by sputtering Si:HfO_2 composite targets [9, 12, 13]. In this approach, the Si content in the film is fixed by the target composition. Therefore, preparing the films with different Si concentrations requires use of multiple targets with varying Si:HfO_2 ratios. In this work, we propose an alternative method based on reactive sputtering in hydrogen-containing plasma. This concept originates from earlier studies on Si-rich SiO_2 films [16], where sputtering a SiO_2 target in an Ar-H_2 atmosphere ("reactive approach") enabled control of the Si content through plasma chemistry. We demonstrate here that a similar strategy can be successfully applied to Si-doped HfO_2. Namely, by sputtering a single composite Si:HfO_2 target in an Ar-H_2 mixed plasma, the Si incorporation in the films can be tuned *in situ* by adjusting the hydrogen flow rate.

The novelty of this work is in demonstrating that hydrogen-assisted reactive sputtering enables dynamic control of the Si content during deposition without the need to modify the target composition. The effects of the deposition parameters – specifically, target composition, substrate temperature, total pressure, and working gas composition (pure Ar or Ar-H_2 mixture) – on the optical and structural properties of Si-doped HfO_2 films are systematically investigated. The obtained results for Si-doped films prepared using this reactive approach are compared with those for undoped and conventionally Si-doped HfO_2 counterparts grown in pure Ar plasma.

2. Experimental details

Undoped and Si-doped HfO_2 films were grown on 2-inch Si substrates (*p*-type, B-doped, 15 Ω·cm, orientation (100)) by radio-frequency (RF) magnetron sputtering of a pure HfO_2 target or composite Si-HfO_2 one, respectively (Fig. 1). The composite target was prepared by placing calibrated Si chips along the erosion track of a 4-inch HfO_2 target (Fig. 1b). The number of the Si chips was varied to cover 3–12% of the target surface. This ratio was defined as $x_{Si} = A_{Si}/A_{HfO_2}$, where A_{Si} and A_{HfO_2} are the surface areas of the Si chips and the HfO_2 target, respectively. Hereafter, the samples grown with $x_{Si} = 0…0.12$ are discussed in detail.

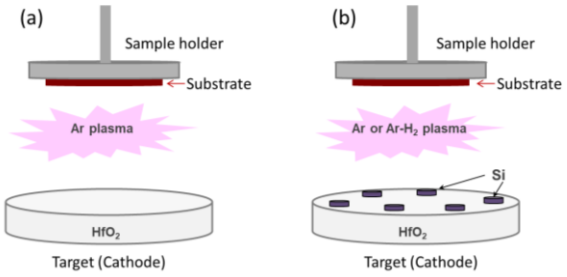

Fig. 1. Schematic presentation of the "bottom-up" deposition process of pure HfO_2 (a) and Si-doped HfO_2 films (b).

Prior to deposition, the Si substrates were cleaned in a 10% diluted hydrofluoric acid solution to remove the Si oxide layer. After cleaning and drying in a nitrogen flow, each substrate was immediately transferred to the vacuum load-lock chamber of the sputtering system.

The RF power density applied to the cathode was fixed at $RFP = 0.74$ W/cm^2. The substrate temperature T_S varied in the range of 45…500 °C. The total pressure during deposition was maintained at $P_{total} = 0.02$ or 0.04 mbar. The total gas flow (Ar and H_2) was 5 sccm, and the hydrogen fraction r_H was defined as the ratio of the hydrogen flow to the total gas flow.

Optical and structural properties of the films were investigated using several complementary techniques. Spectroscopic ellipsometry measurements were performed using a Jobin-Yvon UVISEL system. The spectra were recorded in the 1.5…4.5 eV range at an incident angle of 66.3°, and the data were fitted using DeltaPsi2 software [17]. The accuracy of the refractive index (n) determination was $\Delta n = \pm 0.01$.

X-ray diffraction (XRD) analysis was performed using a Philips X'PERT PRO MDR diffractometer with a $Cu_{K\alpha}$ radiation (λ = 0.154 nm) in a grazing incidence geometry with a fixed angle of 0.5°.

Transmission Fourier-transform infrared (FTIR) spectra were recorded in the 400…4000 cm^{-1} range using Thermo Nicolet Nexus 750 and Shimadzu IRTracer-100 spectrometers. The spectral resolution was 1 cm^{-1}.

Transmission electron microscopy (TEM) was employed to examine the microstructure of the samples. Thin foils were prepared using a standard thinning procedure, which included mechanical grinding, dimpling, and final thinning by Ar ion milling until electron transparency was achieved. Both conventional TEM and high-resolution TEM (HRTEM) were performed using a JEOL FEG 2010 microscope operating at 200 kV. Digital image acquisition and post-processing were carried out using Gatan DigitalMicrograph software.

Auger electron spectroscopy (AES) studies were conducted using a JEOL JAMP-9500F Auger microprobe, providing a spatial resolution of about 3 nm in secondary electron imaging mode. The system was equipped with a hemispheric Auger spectrometer offering an energy resolution ($\Delta E/E$) of 0.05-0.6%, and an ion etching gun for depth profiling. The Ar^+ ion beam had a diameter of about 120 μm and was scanned over a 1×1 mm^2 area.

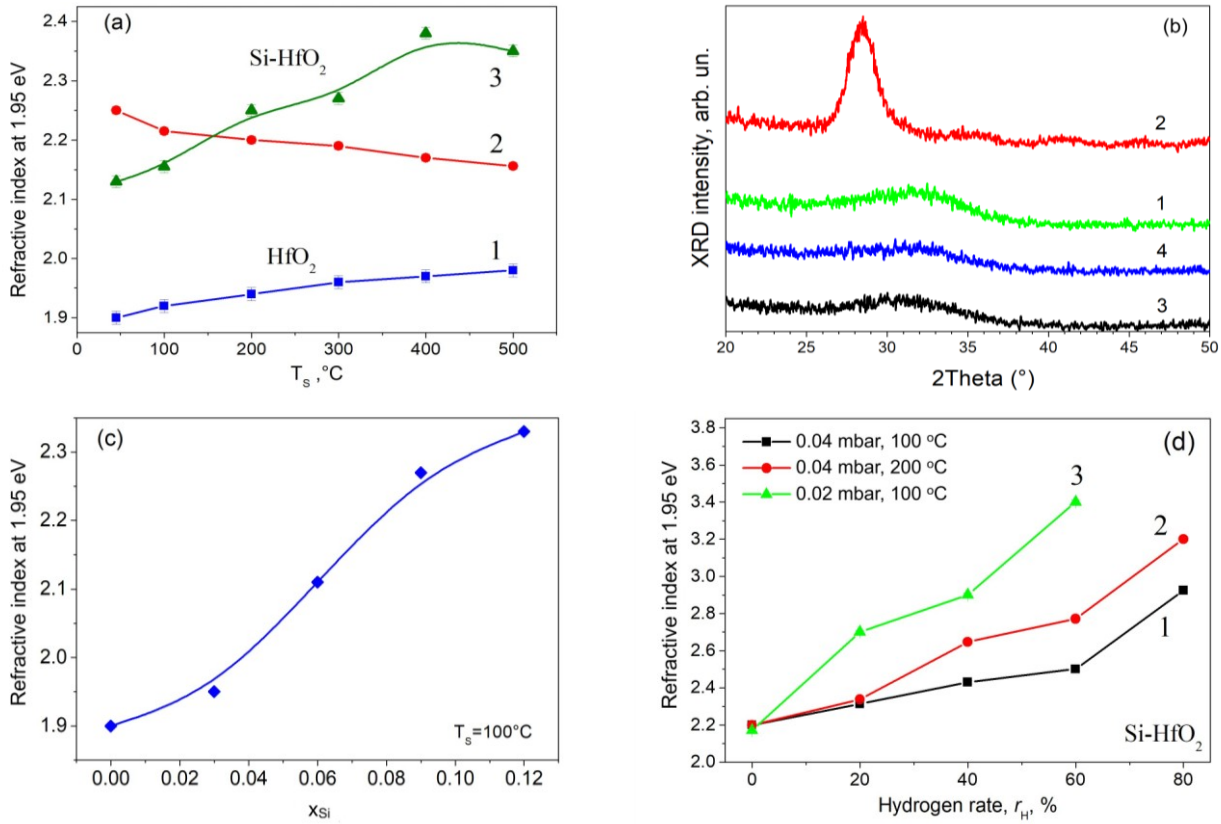

Fig. 2. (a) Variation of refractive index with T_S, for pure HfO_2 (*1*) and Si-doped HfO_2 films (*2,3*) grown in pure Ar (*1, 2*) and Ar-H_2 mixed plasma (*3*); (b) XRD patterns for pure HfO_2 (*1*, *2*) and Si-doped ($x_{Si} = 0.12$) films (*3*, *4*) grown in pure Ar (*1–3*) and in Ar-H_2 mixed plasma (4) at T_S = 100 (*1*) and 500 °C (*2–4*), $P_{total} = 0.04$ mbar; (c) Evolution of refractive index with x_{Si}, $T_S = 100$ °C, $P_{total} = 0.04$ mbar; (d) Effect of hydrogen fraction r_H on the optical properties of Si-doped films deposited at T_S =100 °C (*1*, *3*) and 200 °C (*2*) and $P_{total} = 0.04$ mbar (*1*, *2*) and 0.02 mbar (*3*).

The Ar^+ ion energy ranged from 0.01 to 4.0 keV, with a beam current of 2.0 μA at 3.0 keV. The specimen chamber was maintained under high vacuum ($< 5 \cdot 10^{-7}$ Pa). To minimize charging effects arising from dielectric nature of the samples, a thermal drift correction procedure was applied during spectra acquisition. Quantitative element analysis was conducted by calibrating relative sensitivity factors (RSFs) using homogeneous reference samples of known compositions. All the measurements were carried out at room temperature.

3. Results and discussion

3.1. Effect of deposition conditions on optical and structural properties of the films

The effect of deposition conditions on the optical properties of the films was investigated by spectroscopic ellipsometry. The ellipsometry data for all the samples were fitted using the approach described in [9]. Variation of the refractive index (n) with the deposition conditions was analyzed at the photon energy of 1.95 eV.

Figure 2a presents the evolution of the refractive index for pure HfO_2 films as well as for Si-doped films prepared using different deposition approaches. For the pure HfO_2 films, the n value increases with the substrate temperature T_S (curve *1*). This behavior originates from film crystallization during deposition on substrates maintained at elevated T_S, similar to the results reported in [14].

XRD analysis of the same films confirms their crystallization at higher T_S (Fig. 2b). The films grown at $T_S \leq 100$ °C exhibit a broad XRD peak near $2\theta \sim 31.8°$, characteristic of an amorphous structure (Fig. 2b, curve *1*). Appearance of the sharp (−111) reflection near $2\theta \sim 28.4°$ for $T_S = 500$ °C (Fig. 2b, curve *2*) provides clear evidence of film crystallization in monoclinic phase [18]. These results are consistent with those reported in [10, 15].

The XRD study of the Si-doped films prepared using both deposition approaches revealed their amorphous nature even after deposition at elevated T_S (Fig. 2b, curves *3* and *4*). However, their optical characteristics are substantially different. For the Si-doped films deposited in pure Ar plasma, the refractive index decreases from $n = 2.25$ to 2.15 as T_S rises from 45 °C to 500 °C (Fig. 2a, curve *2*). For the Si-doped films grown using the reactive approach, the refractive index increases to $n = 2.42$ for $T_S = 500$ °C (Fig. 2a, curve *3*). In the former case, the observed decrease in the refractive index may be attributed to the contribution of the phases with lower refractive indices, such as silicon monoxide ($n(SiO) = 2.2$) or dioxide ($n(SiO_2) = 1.46$) as well as voids ($n = 1$).

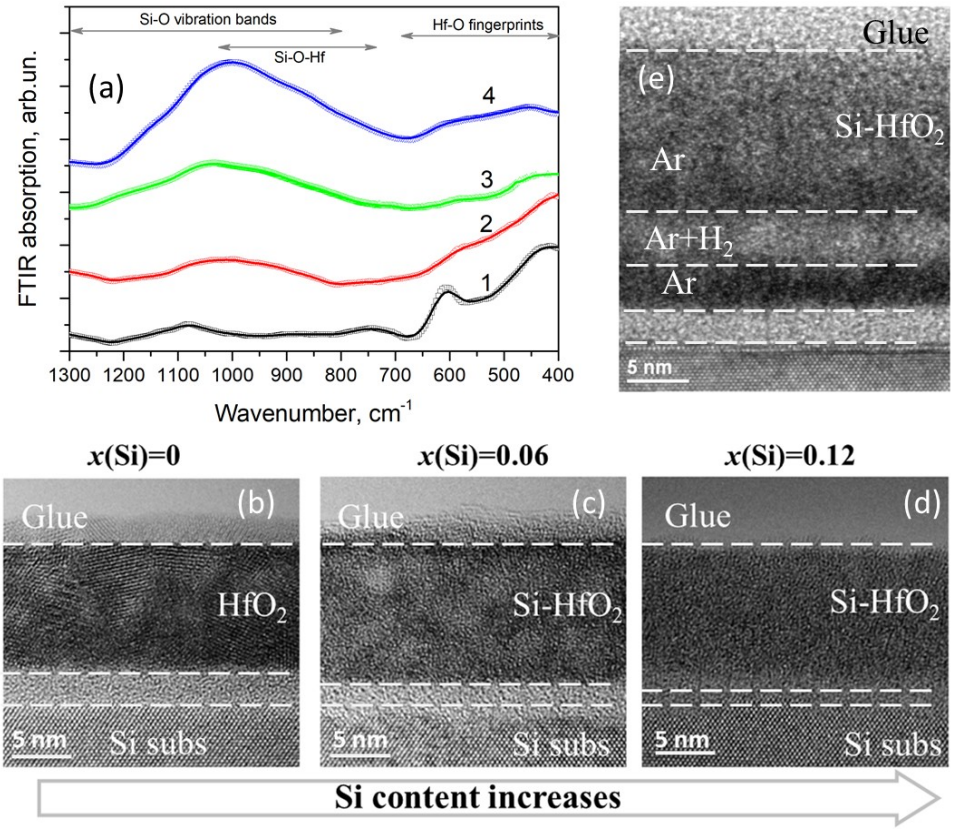

Fig. 3. (a) FTIR spectra of pure (*1*) and Si-doped (*2–4*) films grown in pure Ar plasma (*1–3*) and in Ar-H_2 mixed plasma (*4*). T_S = 400 °C, x_{Si} = 0.06 (*2*) and 0.12 (*3*, *4*); (b–e) TEM cross-section images of the same films grown in pure Ar plasma (*b–d*) and in Ar-H_2 mixed plasma (*e*).

Conversely, for the Si-doped films grown by the reactive approach, the n increase suggests presence of a phase with the refractive index higher than that of HfO_2, possibly related to partly oxidized Si species.

Since the Si-doped films are amorphous, consistent with our earlier results [9], the effective medium approximation can be applied to model their optical characteristics, assuming that these films are composed of Hf- and Si-related structural units.

Typically, Si-doped HfO_2 films are described as a random mixture of HfO_2 and SiO_2 building blocks, forming a solid solution of the type $(HfO_2)_{1-y}(SiO_2)_y$. In such a system, increasing the Si content should rise the fraction of SiO_2 units and, consequently, reduce the refractive index from $n(HfO_2) = 1.98$ to $n(SiO_2) = 1.46$. However, in the present study, the refractive indices of the Si-doped films exceed those of the undoped counterparts prepared under the same conditions. This observation indicates presence of the phase with a higher refractive index, possibly corresponding to monoxide (SiO) ($n = 2.11$) or substoichiometric Si suboxide with [O]/[Si] < 1, whose refractive indices can range between 2.11 and 4.2.

If we consider that the films are made up by HfO_2 and SiO structural units, the n values fall in the range $n = 1.98…2.11$ approaching the higher value with increasing Si content. For our Si-doped films, rise of the Si content in a Si:HfO_2 target results in a significant rise of the n values (Fig. 2c). For instance, at $T_S = 100$ °C, $n = 2.32$ is reached for $x_{Si} = 0.12$ in the films deposited in pure Ar plasma (Fig. 2a,c). It can be inferred therefore that not only Hf-O and Si-O bonds but also Hf-O-Si and Si-Si bonds are formed within the volume of the Si-doped films, indicating presence of excess silicon due to its incomplete oxidation during deposition process. This conclusion is supported by registration of weak absorption in the UV-Vis spectral range (not shown hear) similar to the results of [12], which contrasts with the transparent nature of $(HfO_2)_{1-y}(SiO_2)_y$ solid solution.

The presence of partly non-oxidized silicon is also supported by the variation of the refractive index with hydrogen flow (Fig. 2d). For the samples grown at $T_S = 100$ °C, it varies from $n = 2.25$ ($r_H = 20\%$) to $n = 2.91$ ($r_H = 80\%$) (Fig. 2d, curve *1*). At the same time, reactive deposition at higher T_S results in even higher n values, up to 3.2 (curve *2*). Further increase up to 3.4 was obtained for the films grown at lower r_H and lower total pressure P_{total} (curve *3*). It should be noted that increasing r_H and decreasing P_{total} lead to reduction of the film growth rate by several times. This fact should be considered when optimizing the deposition process.

FTIR spectra further confirm these structural trends. For the pure HfO_2 films grown at $T_S = 400$ °C, a well-defined peak appears near 610 cm^{-1} together with a broad band in the range of 400…500 cm^{-1} (Fig. 3, curve *1*)

testifying partial crystallization of the films [8, 13]. In the Si-doped films ($x_{Si} = 0.06$) deposited in pure Ar plasma, a broad featureless vibration band in the 400…600 cm^{-1} spectral range is observed, being characteristic of amorphous HfO_2-based materials (Fig. 3, curve *2*). At the higher Si content ($x_{Si} = 0.12$), a distinct feature between 800 and 1200 cm^{-1}, which may be attributed to overlapping Si-O and Hf-O-Si vibration bands [9, 13], appears in addition to the broad Hf-O band (400…800 cm^{-1}). For the Si-doped films grown in Ar-H_2 plasma, this high-frequency band becomes more pronounced, indicating an increased Si content in the films. The featureless shape of the FTIR spectra presented in Fig. 3 by curves *3* and *4* is an evidence of the amorphous nature of these Si-doped films.

These spectral peculiarities are consistent with the microstructural changes revealed by TEM observations of the same samples (Figs. 3b–3e). The crystalline planes visible in Fig. 3b indicate formation of HfO_2 grains, while the distinct contrast observed within the film volume is attributed to its porosity. The Si-doped films exhibit an amorphous structure (Figs. 3c–3e). The light gray regions in Fig. 3c may result from both porosity and the formation of Si-rich phases. In Fig. 3d, the uniform grayscale contrast across the film volume evidences a dense film with homogeneous composition. These findings are consistent with the ellipsometry and XRD results (Fig. 2). It should be also noted that for all the samples, formation of a SiO_x interfacial layer between the HfO_2-based film and the substrate was observed.

An amorphous structure was likewise revealed for the films grown in Ar-H_2 plasma (Fig. 3e). This figure also demonstrates feasibility of fabricating films with variable Si content by alternating sputtering of a Si:HfO_2 target of a fixed composition in pure Ar and Ar-H_2 plasmas. The entire film remains amorphous, showing grayscale variations due to compositional changes. Chemical composition was analyzed using the AES method. It was revealed that the Si-doped films grown at 400 °C by sputtering of a Si:HfO_2 target with $x_{Si} = 0.12$ in Ar plasma had a composition Hf:Si:O = 0.33:0.11:0.56, whereas those deposited in Ar-H_2 plasma had the composition Hf:Si:O = 0.34:0.18:0.48. These results indicate that introduction of hydrogen provides an effective approach to control the Hf, Si, and O contents in the films, enabling fabrication of Si-doped HfO_2-based materials with tunable composition. Therefore, analysis of the data described above showed that the optical properties and the film structure can be effectively tuned by controlling the deposition parameters.

3.2. Film microstructure and formation mechanism

The microstructural evolution of the Si-doped HfO_2 films can be interpreted in the framework of the Thornton's structure zone model [6, 7] and its subsequent refinements [18–21]. According to these models, the morphology of sputter-deposited films is primarily governed by the normalized substrate temperature T_S/T_m and the working gas pressure (Fig. 4). The estimation of the T_S/T_m values for Si and HfO_2 is shown in Fig. 4a. The structure zone model (SZM) adopted from [6, 7] is presented in Fig. 4b.

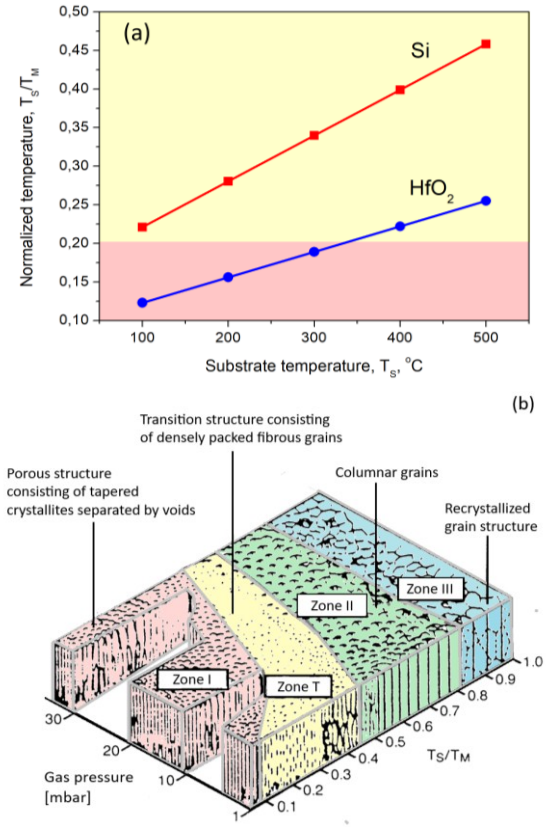

Fig. 4. (a) Variation of the normalized temperature (T_S/T_M) for the component of composite Si:HfO_2 target. The range $T_S/T_m < 0.2$ corresponding to Zone I is highlighted in pink, while the range $T_S/T_m > 0.2$ is highlighted in yellow (Zone T); (b) Schematic presentation of the structure–zone model for sputtered materials as a function of T_S/T_m and working gas pressure, adapted from [6, 7]. Although originally developed for high-pressure sputtering systems, this model remains applicable to low-pressure deposition processes taking place at discharge pressures below 0.05 mbar [18, 19].

At low normalized temperatures ($T_S/T_m < 0.2$, Zone 1), the adatom mobility is limited, leading to porous, fibrous, or columnar growth with a high void fraction. As T_S/T_m increases to 0.25…0.45 (Zone T), surface diffusion becomes sufficient to promote island coalescence and formation of dense, amorphous or nanocrystalline domains. At higher $T_S/T_m > 0.5$ (Zone 2), adatoms have high mobility, resulting in dense, equiaxed grains and smooth film surfaces.

Thornton further refined the model by considering the effect of gas pressure during deposition [6, 7]. At elevated pressures, the kinetic energy of the ions arriving at the substrate and the mean free path of the particles become crucial factors. Depending on this kinetic energy, the degree of ion bombardment of the substrate surface may either increase or decrease, thereby influencing the mobility of the adsorbed atoms. A "transition" zone (Zone T) was therefore introduced between Zone 1 and Zone 2, where the dense film with low porosity and small grain sizes (or even amorphous structure) can form. In our experiments, Zone T can be observed at $T_S/T_m \approx 0.25…0.45$ and working pressures of 0.02 to 0.04 mbar used in the present study.

It should be noted that the Thornton's original structure zone model was developed for high-pressure sputtering and thermal evaporation conditions (10…30 mbar) [6, 7], where the mean free path of atoms is very short and gas scattering dominates the growth. However, in modern low-pressure magnetron sputtering (0.01…0.05 mbar), the deposition conditions differ significantly: the mean free path of the sputtered atoms is much longer, and energetic ion bombardment from the plasma plays a more pronounced role. As a result, the boundaries between Zone 1, Zone T, and Zone 2 shift toward lower substrate temperatures and lower pressures compared to the original diagram. For example, porous or fibrous films characteristic of Zone 1 can appear at discharge pressures below 0.5 Pa (~0.005 mbar) [18, 19], much lower than the Thornton's original values. Therefore, when applying the structure zone model to our HfO_2 and Si-doped HfO_2 films, the pressure axis should be interpreted qualitatively, acknowledging that absolute pressure values are substantially lower than those in the original model [6, 7]. This approach allows us to retain the general concepts of adatom mobility, densification, and amorphization, while correctly situating our low-pressure deposition experiments within the SZM framework.

Taking into account the normalized temperatures for HfO_2 and Si (Fig. 4a), one can infer that the growth mechanism for HfO_2 and Si may differ even at the same substrate temperature. Indeed, the XRD data (Fig. 2b) confirm that pure HfO_2 films tend to crystallize under these conditions, while pure Si films deposited at 100…500 °C typically remain amorphous. Sputtering of a Si:HfO_2 target with low Si content likely results in formation of an inhomogeneous microstructure dominated by isolated HfO_2 and SiO_x clusters. Increasing the Si content in the target enhances the Si fraction in the plasma, and, consequently, incorporation of the Si-related species into the films.

Considering the standard molar Gibbs energy of formation at normal conditions for HfO_2 and SiO_2 (–1088.2 and –856.3 kJ/mol, respectively [22]), formation of HfO_2 is thermodynamically more favorable during deposition. This implies that a significant portion of Si remains only partially oxidized. Deposition of Si-doped HfO_2 films at higher substrate temperatures (T_S = 400…500 °C) can promote a more homogeneous growth of both Hf- and Si-related phases, leading to amorphous films composed of randomly distributed Hf-O and Si-O bonds. A deficiency of oxygen can further favor formation of Hf-O-Si linkages, and this effect becomes more pronounced at higher Si content. An increased Si content in plasma stimulates formation of a larger amount of Si-O bonds and facilitates their incorporation into the growing film, resulting in formation of a mixed Hf-O-Si framework.

Deposition in Ar-H_2 plasma further increases the Si content in the films as confirmed by the ellipsometry data (Fig. 2) and AES analysis. Hydrogen plays a dual role: it reduces the mean free path of plasma ions (light H_2 species increase scattering) and decreases the effective oxygen concentration available for oxidizing Si and Hf. This reductive effect favors partial oxidation of Si, while HfO_2 formation remains energetically preferred. The reduced mean free path and kinetic energy of the Hf and Si ions in presence of hydrogen [7, 18, 19] promote formation of dense amorphous films consisting of Hf-O, Hf-O-Si, Si-O, and even Si-Si bonds, as evidenced by the overall refractive index ($n \approx 2.3…3.2$) and XRD data (Fig. 2). The FTIR analysis (Fig. 3) also supports these conclusions.

It should be pointed out that in [6, 7], the gas pressure during deposition was in the range of 10–30 mbar, whereas in [18–21] it was much lower, around 0.5 Pa (0.005 mbar). In our experiments, the films were deposited at intermediate pressures of 0.02…0.04 mbar. Considering the results of the structural characterization, we can reasonably extend the SZM model to lower pressure regimes. Under these conditions, the mean free path of sputtered particles becomes comparable to or even exceeds the target–substrate distance, resulting in a more directional flux of the energetic species and an enhanced adatom mobility on the substrate surface. In this regard, the Zone T region may be extended to higher substrate temperatures (T_S = 400…500 °C), demonstrating that dense amorphous or fine-grained Si-doped HfO_2 films (depending on the Si content) can still form within this broadened transition zone (Fig. 4b). Such behavior indicates that even at relatively low pressures, interplay between surface diffusion and ion bombardment can effectively compensate the reduced gas-phase scattering, promoting film densification without full crystallization.

4. Conclusions

In this work, we demonstrated successful fabrication of pure and Si-doped HfO_2 films by magnetron sputtering. Increasing the Si content results in formation of homogeneous films with a refractive index higher than that of pure HfO_2, and deposition in argon–hydrogen plasma allows its further increase. It was found that the microstructure, composition, and optical properties of the as-deposited HfO_2-based thin films can be systematically controlled through the target composition, substrate temperature, and plasma environment. Incorporation of Si, especially in combination with hydrogen in the sputtering plasma, promotes formation of dense amorphous Si-doped HfO_2 films with tunable refractive indices while maintaining chemical uniformity. The extended structure–zone model provides a consistent framework to interpret the observed film morphologies, linking adatom mobility, ion bombardment, and densification to the deposition conditions. These results offer a pathway for tailoring the optical properties of high-index amorphous dielectric films in low-pressure magnetron sputtering processes.

Acknowledgements

This work was partly supported by the National Academy of Sciences of Ukraine and Ministry of Education and Sciences of Ukraine. All the TEM results reported in this manuscript fall within the scope of the research foundation IRMA (FR 3095). L.K. thanks for the support via the Program "NADIYA" (2025 edition) implemented by the French Embassy in Ukraine together with the CDEFI (France).

References

1. He G., Zhu L., Sun Z. *et al.* Integrations and challenges of novel high-k gate stacks in advanced CMOS technology. *Progr. Mater. Sci.* 2011. **56**. P. 475–572. https://doi.org/10.1016/j.pmatsci.2011.01.012.
2. Khoshman J.M., Kordesch M.E. Optical properties of a-HfO_2 thin films. *Surf. Coat. Technol.* 2006. **201.** P. 3530–3535. https://doi.org/10.1016/j.surfcoat.2006.08.074.
3. Ansari M.Z., Janicek P., Park Y.J. *et al.* Preparation of wafer-scale highly conformal amorphous hafnium dioxide thin films by atomic layer deposition using a thermally stable boratabenzene ligand-containing hafnium precursor. *Appl. Surf. Sci.* 2023. **620**. https://doi.org/10.1016/j.apsusc.2023.156834.
4. Armellini C., Chiappini A., Chiasera A. *et al.* Rare Earth-activated silica-based nanocomposites, *J. Nanomater.* 2007. **2007**. P. 1–6. https://doi.org/10.1155/2007/84745.
5. Lysaght P., Foran B., Stemmer S. *et al.* Thermal response of MOCVD hafnium silicate. *Microelectron. Eng.* 2003. **69**. P. 182–189. https://doi.org/10.1016/s0167-9317(03)00295-8.
6. Thornton J.A. Influence of apparatus geometry and deposition conditions on the structure and topography of thick sputtered coatings. *J. Vac. Sci. Technol.* 1974. **11.** P. 666–670. https://doi.org/10.1116/1.1312732.
7. Thornton J.A. The microstructure of sputter-deposited coatings, *J. Vac. Sci. Technol. A*. 1986. **4**. P. 3059–3065. https://doi.org/10.1116/1.573628
8. Khomenkova L., Dufour C., Coulon P. *et al.* High-k Hf-based layers grown by RF magnetron sputtering. *Nanotechnology*. 2010. **21.** P. 095704. https://doi.org/10.1088/0957-4484/21/9/095704.
9. Khomenkova L., Portier X., Cardin J., Gourbilleau F. Thermal stability of high-k Si-rich HfO_2 layers grown by RF magnetron sputtering. *Nanotechnology*. 2010. **21.** P. 285707. https://doi.org/10.1088/0957-4484/21/28/285707.
10. Ramana C.V., Vargas M., Lopez G.A. *et al.* Effect of oxygen/argon gas ratio on the structure and optical properties of sputter-deposited nanocrystalline HfO_2 thin films. *Ceram. Int.* 2015. **41.** P. 6187–6193. https://doi.org/10.1016/j.ceramint.2014.12.141.
11. Das K.C., Ghosh S.P., Tripathy N. *et al.* Evolution of microstructural and electrical properties of sputtered HfO_2 ceramic thin films with RF power and substrate temperature. *Ceram. Int.* 2015. **42**. P. 138–145. https://doi.org/10.1016/j.ceramint.2015.08.038.
12. Khomenkov D., An Y.-T., Portier X. *et al.* Light-Emitting and structural properties of Si-rich HfO_2 thin films fabricated by RF magnetron sputtering. *MRS Proc*. 2013. **1617**. P. 85–91. https://doi.org/10.1557/opl.2013.1169.
13. Khomenkova L., Korsunska N., Labbé C. *et al.* The peculiarities of structural and optical properties of HfO_2-based films co-doped with silicon and erbium. *Appl. Surf. Sci.* 2018. **471**. P. 521–527. https://doi.org/10.1016/j.apsusc.2018.11.251.
14. Wiatrowski A., Obstarczyk A., Mazur M. *et al.* Characterization of HfO_2 optical coatings deposited by MF magnetron sputtering. *Coatings*. 2019. **9**. P. 106. https://doi.org/10.3390/coatings9020106.
15. Gao J., He G., Deng B. *et al.* Microstructure, wettability, optical and electrical properties of HfO_2 thin films: Effect of oxygen partial pressure. *J. Alloys Compd.* 2015. **662**. P. 339–347. https://doi.org/10.1016/j.jallcom.2015.12.080.
16. Gourbilleau F., Portier X., Ternon C. *et al.* Si-rich/SiO_2 nanostructured multilayers by reactive magnetron sputtering. *Appl. Phys. Lett.* 2001. **78**. P. 3058–3060. https://doi.org/10.1063/1.1371794.
17. http://www.horiba.com/scientific/products/ellipsometers/software/
18. Joint Committee on Powder Diffraction Standards (JCPDS) No. 78-0050.
19. Guenther K.H. Revisiting structure-zone models for thin-film growth. *Proc. SPIE*. 1990. **1324**. P. 2–12. https://doi.org/10.1117/12.22411.
20. Kusano E. Revisitation of the structure zone model based on the investigation of the structure and properties of Ti, Zr, and Hf thin films deposited at 70–600 °C using DC magnetron sputtering. *J. Vac. Sci. Technol. A*. 2018. **36**. P. 041506. https://doi.org/10.1116/1.5036555.
20. Kusano E. Homologous substrate-temperature dependence of structure and properties of TiO_2, ZrO_2, and HfO_2 thin films deposited by reactive sputtering. *J. Vac. Sci. Technol. A*. 2019. **37**. P. 051508. https://doi.org/10.1116/1.5100307.
21. Abegunde O.O., Akinlabi E.T., Oladijo O.P. *et al.* Overview of thin film deposition techniques. *AIMS Mater. Sci.* 2019. **6**. P. 174–199. https://doi.org/10.3934/matersci.2019.2.174.
22. Barin I., Knacke O., Kubaschewski O. Tables. In: *Thermochemical Properties of Inorganic Substances.* Springer, Berlin, Heidelberg. 1977. https://doi.org/10.1007/978-3-662-02293-1_1.

Authors and CV

Dmytro Khomenkov, PhD student at the Mykola Gogol Nizhyn State University. Field of researches: nanocomposite materials, and their characterization with different optical methods (luminescence, infrared spectroscopy, ellipsometry). Author of 2 scientific papers. https://orcid.org/0000-0003-1884-3623

Semyon Ponomaryov, Researcher (part-time) at the Department of Sensory Systems, V. Lashakryov Institute of Semiconductor Physics, NASU. Field of researches: materials science, Auger electron spectroscopy, scanning electron microscopy, energy dispersive X-ray microanalysis. Author of more than 50 scientific publications. E-mail: s.s.ponomaryov@gmail.com https://orcid.org/0000-0003-4548-4275

Xavier Portier, Full Professor at the National Graduate School of Engineering of Caen (École Nationale Supérieure d'Ingénieurs de Caen, ENSICAEN, Caen, France). His scientific interests cover interrelation between microstructure and physical rare-earth-doped transparent conductive oxide materials optoelectronic applications, and structural characterization of materials by transmission electron microscopy. Author of more than 100 papers. https://orcid.org/0000-0002-5361-719X, e-mail: xavier.portier@ensicaen.fr

Lyudmyla Melnichuk, PhD, Associate Professor at the Mykola Gogol Nizhyn State University, Excellence in Education of Ukraine. Author of more than 120 scientific and scientific-methodical works in the field of semiconductor physics, solid state physics, and problems of higher school.
E-mail: lyu.melnichuk@gmail.com
https://orcid.org/0000-0001-5524-5732

Larysa Khomenkova, Doctor of Sciences, Leading Scientist at the Department of Sensory Systems, V. Lashkaryov Institute of Semiconductor Physics, NASU. Author of over 180 scientific publications. The main activity concerns elaboration of multifunctional composite materials for photonics application, catalysis, and alternative energy sources. E-mail: khomen@ukr.net,
https://orcid.org/0000-0002-5267-5945

Fabrice Gourbilleau, CNRS Research Director at the Centre of Research for Ions, Materials and Photonics (CIMAP), Caen, France. His scientific interests cover materials science, optics, and condensed matter physics. Author of 230 scientific papers.
E-mail: fabrice.gourbilleau@ensicaen.fr,
https://orcid.org/0000-0003-3749-9178

Oleksandr Melnichuk, Doctor of Sciences, Professor at the Mykola Gogol Nizhyn State University, Excellence in Education of Ukraine. Author of more than 300 scientific and methodological works in the field of semiconductor and dielectric physics, solid state physics, mathematical modeling, and problems of higher and secondary school. https://orcid.org/0000-0002-6768-8765

Authors' contributions

Khomenkov D.V.: investigation, formal analysis, visualization, funding, writing – original draft.
Ponomaryov S.S.: investigation, resources, formal analysis, validation.
Melnichuk L.Yu.: investigation, visualization, validation.
Portier X.: investigation, resources, formal analysis, validation.
Khomenkova L.Yu.: investigation, validation, funding.
Gourbilleau F.: resources, validation.
Melnichuk O.V.: supervision, investigation, data curation, validation, funding.
All the authors: writing – review & editing.

Вплив хімічного складу мішені та газової плазми на оптичні та структурні характеристики плівок HfO_2, легованих кремнієм

Д.В. Хоменков, С.С. Пономарьов, Л.Ю. Мельничук, X. Portier, Л.Ю. Хоменкова, F. Gourbilleau, О.В. Мельничук

Анотація. Оптичні та структурні властивості тонких плівок HfO_2, легованих Si, були досліджені в залежності від хімічного складу мішені, температури підкладки (100…500 °C) та складу газової плазми. Плівки були нанесені на кремнієві підкладки з орієнтацією (100) методом радіочастотного магнетронного розпилення композитної мішені Si:HfO_2 у аргоновій або аргон-водневій плазмі. Вміст Si у плівках змінювався шляхом регулювання складу мішені, потоку водню та загального тиску у камері. Методами просвічуючої електронної мікроскопії, спектроскопії ІЧ-поглинання, спектральної еліпсометрії та Оже електронної спектроскопії показано, що плівки HfO_2, леговані Si, є щільними, аморфними та однорідними за хімічним складом. При осадженні в плазмі чистого аргону при загальному тиску 0,04 мбар збільшення вмісту кремнію у мішені сприяє утворенню однорідних аморфних плівок з показником заломлення до 2,42 (при 1,95 еВ), що перевищує показник заломлення чистого HfO_2 (1,98 при 1,95 еВ). Реактивне осадження в аргон-водневій плазмі дозволяє підвищити показник заломлення до 2,75 шляхом збільшення частки водню у загальному потоці газів. Показано, що зростання показника заломлення до 3,4 можна досягти за рахунок зниження загального тиску у камері до 0,02 мбар та/або підвищення температури підкладки. Однак останнє приводить до зниження швидкості росту плівки. Застосовано модель структурних зон для інтерпретації залежності морфології плівок від умов осадження, яка враховує рухливість адатомів, іонне бомбардування поверхні підкладки та процес формування однорідної плівки. Новизна цієї роботи полягає в демонстрації того, що реактивне розпилення з використанням водню дозволяє контролювати вміст кремнію у легованих плівках *in situ* під час осадження без необхідності варіації складу мішені. Показано, що варіація режимів напилення дозволяє керувати мікроструктурою та оптичними властивостями плівок HfO_2, легованих Si. Запропоновані підходи відкривають можливість для створення аморфних покриттів на основі легованого HfO_2 з змінним показником заломлення, придатних для мікро- та оптоелектронного застосування.

Ключові слова: HfO_2, легування, кремній, магнетронне розпилення, тонкі плівки, еліпсометрія, спектроскопія ІЧ-поглинання, просвічуюча електронна мікроскопія, Оже електронна спектроскопія.